



Article

New Approaches to Determining the D/H Ratio in Aqueous Media Based on Diffuse Laser Light Scattering for Promising Application in Deuterium-Depleted Water Analysis in Antitumor Therapy

Anton V. Syroeshkin, Elena V. Uspenskaya , Olga V. Levitskaya , Ekaterina S. Kuzmina, Ilaha V. Kazimova, Hoang Thi Ngoc Quynh and Tatiana V. Pleteneva

Department of Pharmaceutical and Toxicological Chemistry, Medical Institute, Peoples' Friendship University of Russia named after Patrice Lumumba (RUDN University), 6 Miklukho-Maklaya St., Moscow 117198, Russia; syroeshkin_av@pfur.ru (A.V.S.); uspenskaya75@mail.ru (E.V.U.); kkuz11@inbox.ru (E.S.K.); kazimova.ilaha96@gmail.com (I.V.K.); ngocquynhyk@gmail.com (H.T.N.Q.); tvplet@mail.ru (T.V.P.)

* Correspondence: levitskayavolha@gmail.com; Tel.: +7-963-676-12-26



Citation: Syroeshkin, A.V.; Uspenskaya, E.V.; Levitskaya, O.V.; Kuzmina, E.S.; Kazimova, I.V.; Quynh, H.T.N.; Pleteneva, T.V. New Approaches to Determining the D/H Ratio in Aqueous Media Based on Diffuse Laser Light Scattering for Promising Application in Deuterium-Depleted Water Analysis in Antitumor Therapy. *Sci. Pharm.* **2024**, *92*, 63. <https://doi.org/10.3390/scipharm92040063>

Academic Editor: Thierry Besson

Received: 4 October 2024

Revised: 22 November 2024

Accepted: 28 November 2024

Published: 2 December 2024



Copyright: © 2024 by the authors. Published by MDPI on behalf of the Österreichische Pharmazeutische Gesellschaft. Licensee MDPI, Basel, Switzerland. This article is an open access article distributed under the terms and conditions of the Creative Commons Attribution (CC BY) license (<https://creativecommons.org/licenses/by/4.0/>).

Abstract: The development of affordable and reliable methods for quantitative determination of stable atomic nuclei in aqueous solutions and adjuvant agents used in tumor chemotherapy is an important task in modern pharmaceutical chemistry. This work quantified the deuterium/prothium isotope ratio in aqueous solutions through an original two-dimensional diffuse laser scattering (2D-DLS) software and hardware system based on chemometric processing of discrete interference patterns (dynamic speckle patterns). For this purpose, 10 mathematical descriptors (d_i), similar to QSAR descriptors, were used. Correlation analysis of bivariate “log d_i —D/H” plots shows an individual set of multi-descriptors for a given sample with a given D/H ratio (ppm). A diagnostic sign (DS) of differentiation was established: the samples were considered homeomorphic if 6 out of 10 descriptors differed by less than 15% ($n \geq 180$). The analytical range ($r = 0.987$) between the upper ($D/H \leq 2$ ppm) and lower ($D/H = 180$ ppm) limits for the quantification of stable hydrogen nuclei in water and aqueous solutions were established. Using the Spirotox method, a «safe zone» for protozoan survival was determined between 50 and 130 ppm D/H. Here, we discuss the dispersive (DLS, LALLS) and optical properties (refractive index, optical rotation angle) of the solutions with different D/H ratios that define the diffuse laser radiation due to surface density inhomogeneities. The obtained findings may pave the way for the future use of a portable, in situ diffuse laser light scattering instrument to determine deuterium in water and aqueous adjuvants.

Keywords: stable nuclides; deuterium-depleted water (DDW) in antitumor therapy; quantitative determination the D/H ratio; isotope analysis; digital speckle pattern interferometry; non-destructive 2D-DLS technique; Spirotox

1. Introduction

An important role in studying the nature of stable nuclei was rightfully assigned to the following scientists: F. Soddy, D. Thomson, and F. Aston. They, in the 1920s, described the structure and properties of oxygen isotopes: ^{16}O , ^{17}O , ^{18}O [1]. In 1932, the Physical Review Journal published an article by H. Urey, reporting for the first time the discovery of a stable, non-radioactive isotope of hydrogen with an additional neutron—deuterium (^2H) (from the ancient Greek *deuteros*—second) [2]. Obtaining D_2O by electrolysis of aqueous solutions gave rise to intensive studies of its properties. All this marked the beginning of the era of stable nuclei, which demonstrated obvious advantages over the radioactive ones: a longer half-life; the ability to determine the D/H ratio by mass spectrometry; stability and an absence of radioactivity, and safety of its use in industry without the need for special

protective measures [3,4]. Moreover, potential adverse health effects of radioactivity in human subjects limited the use of radioactive nuclides. In addition, the versatility of stable isotope methodology greatly expanded the possible studies to be undertaken. However, harnessing them in industry began much later due to the limited availability of suitable isotopes and more complex detection techniques compared to radioactive nuclei [5].

Stable non-radioactive isotopes—tracers—are successfully used in medicine to study the kinetics of human metabolism *in vivo* [6]. The high sensitivity and specificity of tracers allow them to be followed in complex processes of redistribution and transformation of substances, including living organisms. In studies of human metabolism, the most commonly used stable isotopes are nitrogen, hydrogen and oxygen (^{15}N , ^2H and ^{18}O), which can be incorporated into molecules and used as metabolic indicators [7,8]. To this end, one or more stable isotope tracers are injected intravenously into the blood circulation system, which is accompanied by the collection of blood samples before and after the infusion of tracers (Figure 1a).

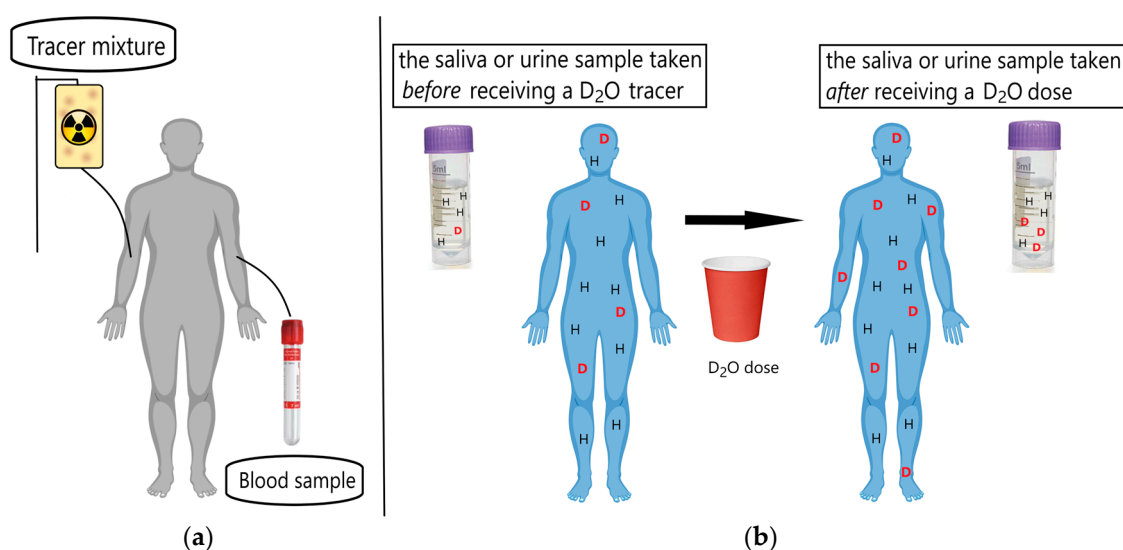


Figure 1. Schematic diagrams of human stable nuclide monitoring: (a) ^{15}N , ^2H и ^{18}O tracers; (b) D_2O tracer.

A metabolic isotope tracer is a molecule that is chemically and functionally identical to the naturally occurring molecule of interest (a tracee). Following the fate of the tracer provides information on the metabolism of the tracee [9]. The isotopic enrichment, as a ratio of tracer to tracee, is determined using gas or liquid chromatography–mass spectrometry (GC/MS or LC/MS) [10].

In recent years, there has been considerable interest in alternative methods of stable isotope labeling, such as deuterium oxide (D_2O or heavy water). The unique properties of this tracer include the possibility of oral administration and flexible control of its flow through various body substrates, unlike ^{15}N , ^2H and ^{18}O tracers (Figure 1b).

Moreover, using D_2O allows for evaluating the turnover of plasma and muscle proteins (e.g., dynamic proteomics) in addition to metabolomics (e.g., fluxomics) to seek molecular underpinnings, e.g., of exercise adaptation [11].

The constancy of the isotopic composition of elements in nature, being associated with the genesis and repeatability of their proportions, is evidenced by the results of many studies [12]. It is known that the stable isotopic composition of drinking water, diet, and atmospheric oxygen affect the isotopic composition of water in the body, which is usually expressed as $\delta^{18}\text{O}$ ($^{18}\text{O}/^{16}\text{O}$) and $\delta^2\text{H}$ ($^2\text{H}/^1\text{H}$) [13,14]:

$$\delta^{18}\text{O} = \left[\frac{(^{18}\text{O}/^{16}\text{O})_{\text{sample}}}{(^{18}\text{O}/^{16}\text{O})_{\text{standard}}} - 1 \right] \cdot 1000 \text{ ‰}, \quad (1)$$

$$\delta^2\text{H} = \left[\frac{(^2\text{H}/^1\text{H})_{\text{sample}}}{(^2\text{H}/^1\text{H})_{\text{standard}}} - 1 \right] \cdot 1000 \text{ ‰}, \quad (2)$$

where $\delta^{18}\text{O}$ ($\delta^2\text{H}$) is the measure of the deviation in ratio of stable isotopes ^{18}O and ^{16}O ($\delta^2\text{H}$ and $\delta^1\text{H}$).

For example, the isotopic composition of stable nuclei in natural water is characterized by a particular constancy: $\text{D}:\text{H} = 1:6000$ and $^{18}\text{O}:^{17}\text{O}:^{16}\text{O} = 1:0.2:500$ [15]. The Global Climate Observing System (GCOS), Switzerland, has used deuterium and oxygen-18 as official climate parameters since 2007. The International Atomic Energy Agency (IAEA) coordinates the isotope measurements worldwide and manages the Global Network of Isotopes in Precipitation (GNIP) and the Global Network of Isotopes in Rivers (GNIR). Existing variations of stable isotopes of hydrogen and oxygen in natural water are normalized by common standards for the isotopic composition of the hydrosphere: SMOW-V, SLAP, and GISP (Table 1) [16].

Table 1. Basic isotopic standards of water with variations in the content of stable atomic nuclei.

The Name of Standard	Reference Value			
	$\delta^2\text{H}$, ‰ *	^2H , ppm	$\delta^{18}\text{O}$, ‰ *	^{18}O , ppm
Vienna Standard Mean Ocean Water (SMOW-V)	0	155.76	0	2005.20
Standard Light Antarctic Precipitation (SLAP)	−427.50	89.00	−55.50	1894
Greenland Ice Sheet Precipitation (GISP)	−189.80	126.20	−24.85	1955.37
Greenland Summit Precipitation (GRESF)	−258.0	−	−33.40	−

* Relative units expressing the content of D and ^{18}O in water molecules and equated with zero: δD , ‰ (or 155.76 ppm), for $\delta^{18}\text{O}$, ‰ (or 2005.20 ppm).

The work assessing variations in human body water isotope composition across the United States [17] showed that the community level variation exists in the $\delta^{18}\text{O}$ ($^{18}\text{O}/^{16}\text{O}$) and $\delta^2\text{H}$ ($^2\text{H}/^1\text{H}$) values and the primary drivers are the regional differences in drinking water isotopes. The consistency of the body water isotope composition over the study period suggests that tissues would incorporate a stable isotope signal over time. The content of individual isotopologues in natural water (H_2^{16}O , H_2^{18}O (0.20%), H_2^{17}O (0.04%), HD^{16}O (0.017%)) is comparable to that of the most important (essential) microelements in seawater and plasma [18]. Deviations from this rule have become important for the observed physicochemical and biological effects of water [19].

Differences in the physicochemical properties of compounds caused by the replacement of one isotope with another are significant only for hydrogen nuclei. This is due to both the twofold difference in the masses of protium and deuterium atoms ($^1\text{H} = \text{p} + \text{e}^-$; $^2\text{H} = \text{p} + \text{n} + \text{e}^-$) and the fundamental relationship between the mass and energy of any body [20], which implies that a change in the mass of a body (ΔM) results from a change in its energy (ΔE):

$$\Delta\text{E} = c^2 \cdot \Delta\text{M}, \quad (3)$$

where c^2 is the square of the speed of light.

For atoms of other elements, the differences in the properties of isotopologues are very small.

Studying the effect of replacing deuterium with protium on the physical properties of water and aqueous solutions is of particular interest since it could cause as well as control significant changes in the constants of both physicochemical processes and biological processes in vitro and in vivo. It was shown [21] that the rate of chemical reactions between substances in the case of replacing D/H may differ by 5–10 times.

Much of the relevant literature has focused on studying the role of deuterium in natural or reduced (see Table 1) content in the human body [22,23]. Any shifts in the D/H balance outside or inside the cells trigger immediate reactions—alteration of pro-

liferation and apoptosis rates [24]. Recent studies have confirmed that ^2H is a natural cell growth regulator responsible for mitochondrial redox balance [25]. Amounting evidence shows that ^2H plays a key role in cell proliferation and energy metabolism [26,27]. Major observations were related to cell growth/differentiation, immune/nervous system responses, endurance/adaptation, mitochondrial electron transfer, energy production, glucose metabolism, etc. [28]. It is reported that water depleted in deuterium by 65% can exhibit antitumor properties, for example, against nasopharyngeal carcinoma (NPC), pancreatic cancer or glioblastoma multiforme (GBM) cells, acting as an effective inhibitor of their proliferation [29–31]. Cell cycle analysis revealed that DDW caused cell cycle arrest in the G1/S transition, reduced the number of cells in the S phase and significantly increased the population of cells in the G1 phase in NPC cells. The inhibitory effect of DDW, especially at concentrations of 30–100 ppm, alone and in combination with antitumor antimetabolites (Fluorouracil (5-FU), Temozolomide (TMZ), and radiation therapy (RT) on Michigan Cancer Foundation-7 (MCF-7) breast cancer and GBM cells, significantly increases the survival rate of patients. Along with cell cycle arrest at the G1/S transition, the activity of superoxide dismutase (SOD) and catalase (CAT) enzymes increases at DDW concentrations below natural (SMOW-V) values [32]. The authors [33] claim that a significant advantage of deuterium-depleted water is that it appears to have no pharmacological side effects, in contrast to current antitumor therapy. Scientists are unanimous in their opinion that supplementing the traditional treatment methods (chemotherapy and radiation therapy) with deuterium depletion adjuvant therapy contributes to a better survival rate of patients at the advanced stages of severe oncological pathologies [34]. The anticancer effect of D depletion was confirmed in a randomized phase 2 clinical trial on prostate cancer [35].

Along with the increased production of deuterium-depleted water for medical purposes (20 ppm, 45 ppm, 65 ppm, 86 ppm) and everyday life (105 ppm, 125 ppm) [36], the development of accessible techniques and methods for screening-quantitative D/H ratio analysis is both timely and topical. The existing technical capabilities for isotope analysis, such as isotope ratio mass spectrometers (IR-MS), Off-Axis Integrated Cavity Output Spectroscopy (OA-ICOS), neutron scattering techniques with H/D isotope labeling, confocal Raman microspectroscopy (CRM), and isotope ratio infrared spectroscopy (IRIS), are associated with various limitations. The existing methods require complex preparation, they are time consuming and expensive, requiring either the destruction of samples during analysis, or yielding low resolution [37–41].

Therefore, the major aim of this study is to substantiate and develop approaches for monitoring stable hydrogen nuclides in aqueous solutions based on an original chemometric processing of the dynamic speckle (DSpc) patterns of back diffuse scattering from the surface of liquid objects for promising applications in deuterium-depleted water analysis for anticancer therapy.

2. Materials and Methods

2.1. Reagents

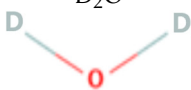
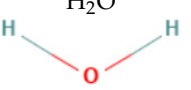
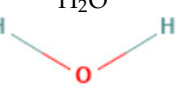
The reagents include the following:

Deuterium oxide D_2O (heavy water, water-d2), for NMR, 99.8 atom % D, D-enrichment $\geq 99.75\%$, Nitrogen flushed, very hygroscopic (Thermo Scientific Chemicals, Waltham, MA, USA) (Table 2) [42].

Water, deuterium-depleted (deuterated depleted water DDW, protium water, “light water”), ≤ 1 ppm deuterium oxide (Sigma-Aldrich, Waltham, MA, USA).

Water bidistilled, Bd (hydrogen oxide, water), conductivity $\kappa < 5$ S/m (Bidistillator-BS, NV-Lab, Moscow, Russia) with natural content of stable hydrogen ^2H nuclear, corresponding to the SMOW-V-standard (see Table 1).

Table 2. Specification of water preparations with variations in stable hydrogen isotope content [43,44].

Specifications	Water Samples		
	heavy water	water bidistilled	light water
Linear Formula +2D			
Molecular Weight, g/mol	20.0276	18.0150	18.0106
Solubility in water	Miscible, exothermic reaction	Completely miscible	Miscible, exothermic reaction
Physical Form	Liquid	Liquid	Liquid
Color	Colorless	Colorless	Colorless
pH	7.4	5.7–7.5	6.0–8.0 **
Refractive Index	1.32844 *	1.33300	1.33335
Viscosity, cP **	1.107	1.012 ****	0.987 ****
Density, g/mL **	1.1056	0.9998	0.9969 ****
Surface Tension, dyn/cm	71.93	71.99	75.17 ****
Melting Point, °C	3.8	0	−1.5 ****
Boiling Point, °C	101.42	99.97 ***	93.70 ****

* 20 °C; ** 25 °C; *** [45]; **** [46].

Study Design

Laboratory test samples with D/H variations from 1 ppm to 264 ppm with an increment of 40 ppm were obtained in situ by serially diluting D₂O with DDW aliquots. Water with a D/H ratio of more than 200 ppm was represented by two samples: 1000 ppm and 1×10^6 ppm (D₂O, 99.8%). To this end, micropipettes with volumes ranging from 0.1 µL to 100 µL were used. To exclude extraneous heterogeneous contaminants in the water samples, filtration was performed through a submicron inert membrane filter (Millex-GV Filter with a 0.22 µm pore size hydrophilic PVDF membrane, Merck Millipore, Burlington, MA, USA).

2.2. Methods

2.2.1. Two-Dimensional Diffuse Laser Scattering (2D-DLS)

The original approach developed in this study is based on a physical phenomenon associated with the impact of femtosecond laser pulses generated by an infrared (IR) emitter with a built-in high spectral density LED on the smooth surface of water samples. To probe the surface of the sample, new-generation LEDs were used (50 mW/cm² λ ~810 nm, spectral line width 2–4 nm), connected to a laptop via a USB port (model AA3528LVBS/D, type C503B-BCN-CV0Z0461, CreeLED, Inc., Huizhou, China), with images captured using Soft Cameratune (Figure 2).

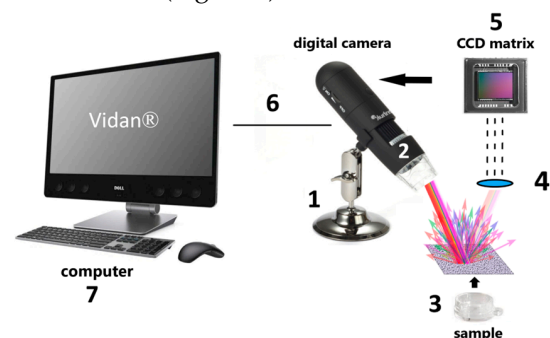


Figure 2. Principal schematic of the equipment for two-dimensional inverse diffuse scattering technique: 1—compact emitter, 2—laser processing module, 3—test sample, 4—collecting lens, 5—charge-coupled device (CCD), 6—USB cable, 7—personal computer.

The resultant intensive photoexcitation from light scattering centers in the surface layer—optical inhomogeneities—that is associated with density fluctuations creates conditions for diffuse reflection and is governed by the Rayleigh criterion:

$$h < \frac{\lambda}{8\cos\varphi}, \quad (4)$$

where h is the height of density inhomogeneities, λ is the wavelength of the incident light, and φ is the angle of incidence on the surface.

According to [47,48], light scattering centers can be described by a transmission matrix (T_M), which reflects the relation between the incident light E_{incident} and the transmitted light $E_{\text{transmitted}}$:

$$E_{\text{transmitted}} = T_M \cdot E_{\text{incident}}, \quad (5)$$

where T_M is deterministic for a given optical configuration.

Diffusers—that is, surface “roughness”—emit spherical waves as secondary light sources when reflecting laser light and, as a result of the interference, the appearance of laser speckles is observed [49]. The emerging speckle structure is represented by the alternating light and dark spots in the image as stretched in time. To capture the DSpc image at a specific frame rate, a special Vidan[®] Software (No. 2005612135, ROSPATENT) was developed (Figure 3).

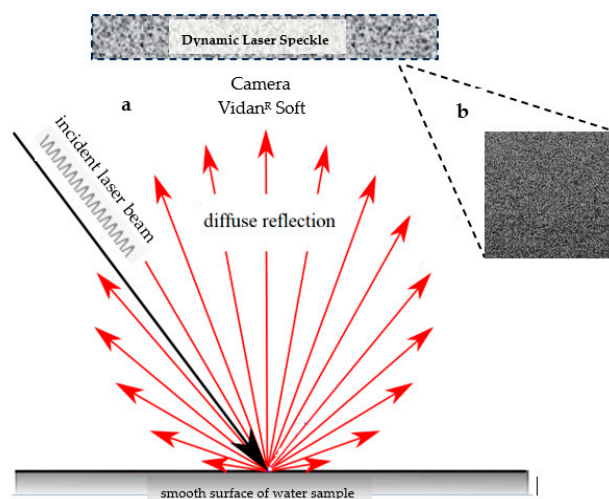


Figure 3. The diffuse laser scattering scheme (a) an optical field incident is scattered by an optical diffuser and imaged by a camera; (b) an area of the captured speckle pattern is created by the laser diode.

The dynamic speckle (DSpc) does not bear any resemblance to the object, but it contains exhausting visual information about the distribution of scatterers in it, since it records the amplitude and phases of the wave field as a result of the superposition of the reference coherent wave and the waves diffracted on the object [50]. Supramolecular density inhomogeneities in water, which are deuterium-stabilized heterophase clusters or the bubston structure of water, can act as scatterers in accordance with the references [51,52].

The resultant DS patterns were further processed chemometrically using the Vidan[®] Software with ten topological descriptors similar to the QSAR descriptors of Wiener (W) and Balaban (J) as modified by Trinajstić (I) (Table 3) [53]. Each descriptor is responsible for the topological convolution of the DS matrix obtained by subtracting the background from each speckle element captured (see Figure 3). Therefore, the descriptor reflects both spatial inhomogeneities on the surface or color, and the dynamic variability of light reflection.

Table 3. Representation of chemometric 2D-DLS descriptors.

Descriptor	Mathematical Representation	Description
d_1	$d_1 = \frac{i_{\Delta Si > Sb}}{i_t} \cdot 100\%$ i_t is the total number of elements. ΔSi is the value of differences in the signal level of the elements of two interference patterns. Sb is the threshold level of the signal.	The number of different elements, regardless of the degree of difference.
d_2	$d_2 = \frac{\sum_{\Delta Si > Sb} \Delta S_i}{i_t \cdot \bar{S}} \cdot 100\%$ $\sum_{\Delta Si > Sb} \Delta S_i$ is the average value of the signal level of all the elements of the original interference pattern.	The degree of difference for each discrete element based on the original interference pattern and the total intensity of the level of its signal.
d_3	$d_3 = \frac{\sum_{\Delta Si > Sb} \Delta S_i}{i_t \cdot \Delta S_{max}} \cdot 100\%$ ΔS_{max} is the sum of maximum possible differences in terms of the signal level of all the relevant elements of the interference patterns of absolute black and absolute white.	The maximum value of possible differences between the interference patterns of absolute black and absolute white.

The d_1 , d_2 , d_3 descriptor family has been expanded to three triads for greater statistical reproducibility: sd_1 , sd_2 , sd_3 (standard deviations); r_1 , r_2 , r_3 ($r_i = d_i/sd_i$); and the R descriptor, which combines all of the above ($R = \prod_i R_i / \sum_i R_i$). A combination of ten descriptors gives a statistically reliable reflection of the degree of difference in the obtained DS interference patterns, which allows for characterizing the object under study based on the nature of its near-surface scatterers.

2.2.2. Study Design

The stages of two-dimensional inverse diffuse scattering technique for stable hydrogen nuclide monitoring in different aqueous solutions included filling the cuvette with a solution of the test sample $V = 700 \mu\text{L}$; laser pumping, that is, transferring LED energy into the working medium with obtaining in situ graphical interpretations of the distribution of descriptors (see Table 3) over time; and scanning is accompanied by high-speed photography (more than 10 frames per second) for 60 s, three parallel measurements with the number of runs ($n = 180$) for each one. The images are captured using a CCD matrix (Figure 4).

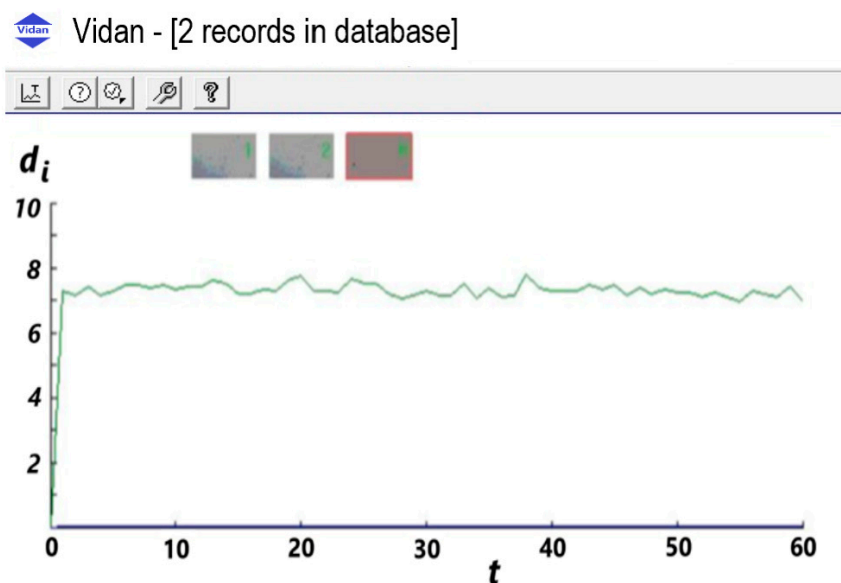


Figure 4. The visualization of the technique for chemometric analysis of dynamic speckle images, presented as the dependence of descriptors d_1 , d_2 , d_3 on the time of accumulation of the DSpc data.

The results are considered reliable when a time-stable result of data accumulation was obtained in d_i - t_{sec} coordinates, which was accompanied by the absence of a significant scatter of data in $sd(d_i)$ — d_i -average (t_{sec}) coordinates. The diagnostic feature (DF) of differentiation was established: samples were considered to be homeomorphic if 6 descriptors out of 10 differed by less than 15% ($n \geq 180$).

2.2.3. Dynamic Light Scattering (DLS)

The size distribution of Lcs particles from 0.1 nm to 1000 nm, their electrokinetic potential and dispersion control in aqueous solutions before and after high-intensity mechanical loading were determined by a ZetasizerNano ZS dynamic light scattering (DLS) spectrometer (MALVERN Instruments, Malvern, UK). The dynamic light scattering method is based on the analysis of fluctuations in the intensity of light scattered by particles in a state of chaotic Brownian motion. As a result of the fluctuation analysis, the diffusion coefficient is determined and the hydrodynamic radius of particles is calculated on the basis of the Stokes–Einstein equation. The Stokes–Einstein equation is as follows:

$$D = \frac{k_B T}{6\pi\mu r_H}, \quad (6)$$

where D is the diffusion coefficient (in the case of spherical particles), μ (Pa·s) is the dynamic viscosity of the medium, and r (mol) is the radius, which can be derived via the molar volume and Avogadro's constant. $T(K)$ is the absolute temperature and $k_B = 1.38065 \times 10^{-23} \text{ J} \cdot \text{mol}^{-1} \cdot \text{K}^{-1}$ is Boltzmann constant.

The DLS method was used to determine the most important quantitative characteristics, Z-average size and Polydispersity Index (PDI).

2.2.4. Static Light Scattering (SLS)

To determine the size distribution of particles and clusters (“size spectrum”) from 1 to 180 μm , we used the laser diffraction technique (Malvern Instruments, Malvern, UK), based on recording the scattering indicatrix that arises during the interaction of electromagnetic radiation with density inhomogeneities in the medium. *N*-Hexane was used as a background.

2.2.5. Determination of the Optical Rotation (OR)

The effect of D/H variations on the optical activity of water samples (hysicum oxide, DDW, water bidistilled) was determined using an Atago POL-1/2 polarimeter (ATAGO Co., Ltd., Tokyo, Japan) in a 100 mm cell, with an accuracy of $\pm 0.002^\circ$ and resolution of 0.0001° . The light source was an LED with interference filter, $\lambda = 589 \text{ nm}$. To establish the required temperature conditions ($20 \pm 0.5^\circ\text{C}$), a Peltier electronic module was used. The blank sample was *n*-hexane (anhydrous, 95%, Sigma-Aldrich, Taufkirchen, Germany). After setting the polarimeter to the zero point, the main measurement of each of the water samples was carried out over a week with $n \geq 1000$ independent experiments. The results obtained were expressed as the dependence of the frequency of occurrence of values on the optical rotation angle.

2.2.6. The Refractive Index (RI) Determines

For high-precision measurements of the refractive index of the studied water samples (accuracy 0.0002) with variations in D/H, a laboratory Abbe refractometer (KOMP, Kazan, Russia) was used at $T = 20 \pm 0.2^\circ\text{C}$ ($n = 3$, $p = 0.95$). The device is equipped with a built-in thermometer, Brix and refractive index (RI) scales, as well as a measuring prism with a liquid sample volume of $V = 0.5 \text{ mL}$.

2.2.7. Spirotox-Method

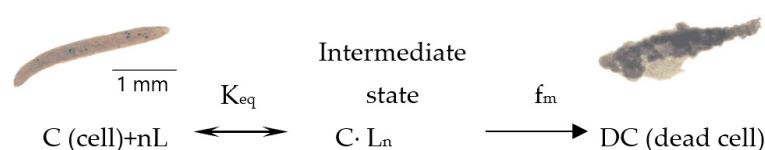
The biological activity/toxicity study of water samples with D/H variations was studies using the Spirotox bioassay method [54].

Ciliated protozoan *Sp. Ambiguum* (3–5 adults) was placed in a thermostated cell filled with different D/H ratio in water sample. The observation of the behavioral response and the recorded time of cell death were marked by successive signs: convulsions—twisting—cessation of motor activity. The temperature (Arrhenius) dependence of the lifetime of *Sp. Ambiguum* was studied ($T = 301\text{--}309\text{ K}$) with subsequent calculation of the observed activation energy of the process of cellular transformations described by the schematic diagram (Equation (7)).

$$K = A_0 \exp\left(-\frac{E_a}{RT}\right). \quad (7)$$

Here, A_0 is the pre-exponential factor, E_a is the energy of dead cell stage (kJ/mol), R is the universal gas constant (8.31 J/mol·K), and T is the temperature (K).

The existence of an intermediate state in the process of ligand-induced death of a subject means that the cell death process must occur at the activation stage with energy expenditure (Scheme 1).



Scheme 1. Kinetic scheme of ligand-receptor *Sp. Ambiguum* interaction: C is cell, L is ligand, n —stoichiometric coefficient, $C \cdot L_n$ —intermediate state (cell after interaction with the ligand), K_{eq} is the equilibrium constant fast stage, f_m is the rate constant of the cell transition to the dead state, DC is a dead cell. The inserts show photographs of ciliates at the stages of incubation in the medium and recorded of death.

2.3. Statistical Data Processing

All statistical data processing was performed using Student's t -test and the Origin Pro 2021 software (OriginLab, Northampton, MA, USA). The differences were considered statistically significant at $p < 0.05$.

3. Results

It was shown earlier that many physicochemical properties of water, including anomalous ones, as well as biological effects of water and aqueous solutions, were associated with variable deuterium concentrations [55–60]. To justify the use of the two-dimensional (2D) diffuse laser light scattering technique in D/H analysis in water samples that are used as well in adjuvant antitumor therapy, it is necessary to understand the properties of surface “scatterers”. Additionally, this section will consistently set forth the issues of the biological effects of water with D/H variations, the validation of the portable device to monitor D/H contents in aqueous solutions and adjuvant therapeutics, as well as the results of possible application of the proposed fast and simple 2D diffuse scattering technique.

3.1. Biological Effects of Deuterium-Depleted Water (Light Water)

Figure 5 shows the effect of water with deuterium content from 1 ppm to 264 ppm on the survival time of the *Spirostomum ambiguum* cellular biosensor under different temperature conditions, followed by calculating the observed activation energy of the process of cellular transitions to an immobilized state (see Scheme 1).

We have found that the dependence of the survival time of the cellular biosensor on the deuterium content in water, which is “dose–response” relations, for water samples with D/H ratio is identical to the physiological classical curves for essential microelements: a lack or excess of a micronutrient leads to the death of the living organism (see Figure 5a,b) [61]. At the same time, there is a so-called “safe zone” that ensures normal survival rates of the organism (see Figure 5c) in the presence of a micronutrient in a certain concentration: the “dose–response” relation curve runs almost parallel to the X-axis in the range of D/H values from 50 ppm to 130 ppm and gradually goes down beyond this range.

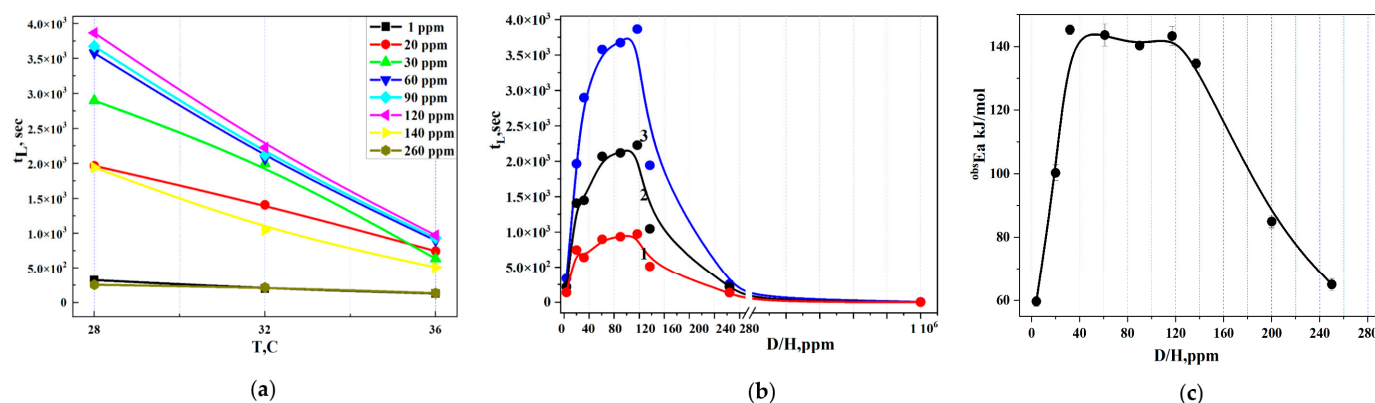


Figure 5. The dependence of *Sp. Ambiguus* lifetime (survival rate) on deuterium concentration in water (a) under the following conditions: (b) at 36 °C (1), 32 °C (2) and 28 °C (3). (c) The “dose—response” relations in observed values of activation energy (values of observed activation energy) ^{obs}Ea.

3.2. The Description of Surface “Scatterers”

The minimum signal-to-noise ratio (SNR) is an important indicator for assessing the reliability of results and their subsequent use to account for the physicochemical properties and biological effects of water in aquatic systems. Figure 6 presents the expanded signal to noise ratio (SNR) estimates for validating the established opinion about the implementation of the isotope effect through the cluster organization of water and density inhomogeneities for the associated liquid [62,63].

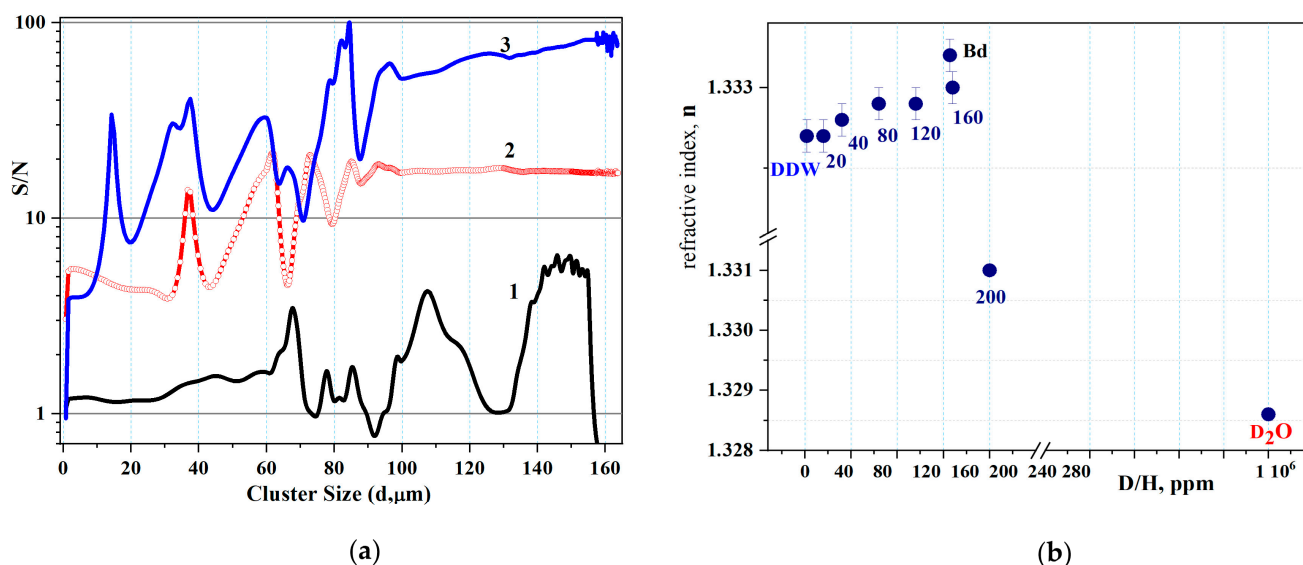


Figure 6. Properties of water with variations in D/H ratio: (a) signal-to-noise ratio (SNR) calculated from measurements for water samples: water bidistilled (SMOW-V) (1); deuterium oxide, 99.8 atom% D (2); water, deuterium-depleted, ≤ 1 ppm (3) by the LALLS data ($n = 15$; $p = 0.95$). $SNR = \frac{\bar{V}}{SD}$, \bar{V} is the average volume fraction (%) of water clusters, SD is standard deviation. The solid horizontal lines denote recommended uncertainty levels (values should be below the lines), and (b) the refractive index (RI) dependence on the deuterium content in water.

The graph shows a downward trend for the noise level in Bd water with natural (SMOW-V) deuterium content, thereby providing a minimum threshold for statistically significant data. The DDW sample (see Figure 6a (3)) shows a higher SNR compared to D₂O (see Figure 6a (2)), but without reaching the threshold value.

The refractometric index (RI) values increase with growing deuterium content in water up to natural values corresponding to the SMOW-V standard. The subsequent increase in

deuterium content above the SMOW-V standard is accompanied by a drop in the RI value and reaching a minimum in the D₂O medium (in the absence of protium) (see Figure 6b). The results obtained correspond to the “dose–response” relationships and thus reflect the nature of the emerging density inhomogeneities that affect the properties of water and aqueous solutions.

The effect of D/H variations on the properties of its aqueous solutions was studied using the example of changes in such physical-chemical properties as the hydrodynamic radius of density heterogeneities (d , nm), the values of count rate (CR) and the polydispersity index (PDI) (Figure 7).

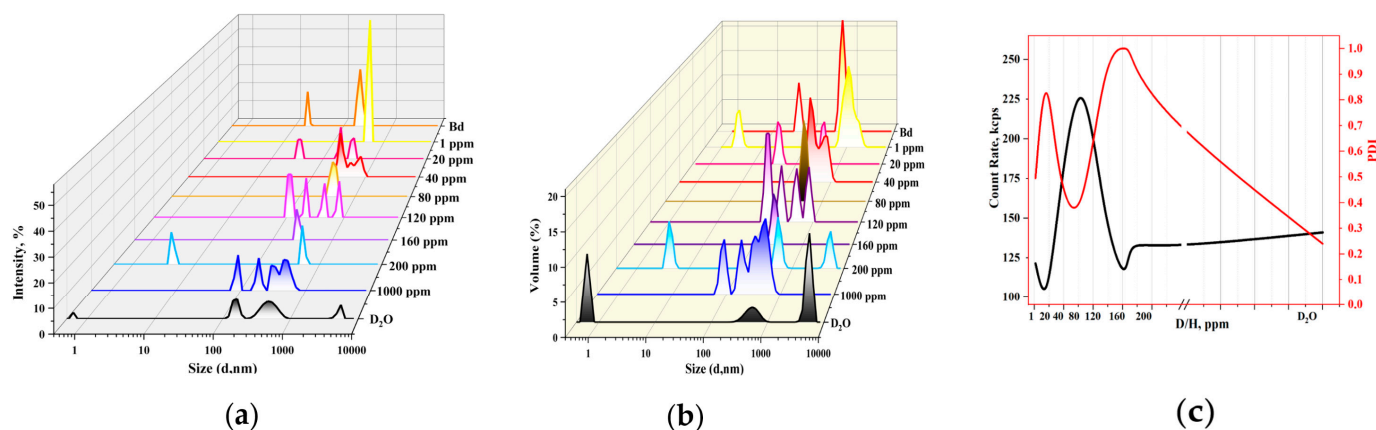


Figure 7. Particle size distributions (PSD) of density heterogeneities (water clusters) in D/H different samples in units: (a) laser light scattering intensity; (b) volume concentration; (c) count rate and PDI.

Noteworthy is the range of water cluster sizes from 100 nm to 1000 μ m with the highest distribution density of water samples with D/H variations and characteristic maxima in units of intensity and volume. The counting rate defined as the number of photons registered per second by the detector is inversely dependent on the polydispersity index (PDI) for the studied samples with different D/H ratios. The CR value minima and PDI maxima correspond to samples DDW, Bd, sample D/H = 160 ppm and D₂O, which indicates a higher dispersity for these objects of study.

The possibility of spontaneous formation of stable alternating chiral hierarchies in water structures was stated in [64]. We have demonstrated differences between DDW, Bd and D₂O water samples in fluctuations in optical rotation angle values as a function of the relative frequency of occurrence (Figures 8 and S1).

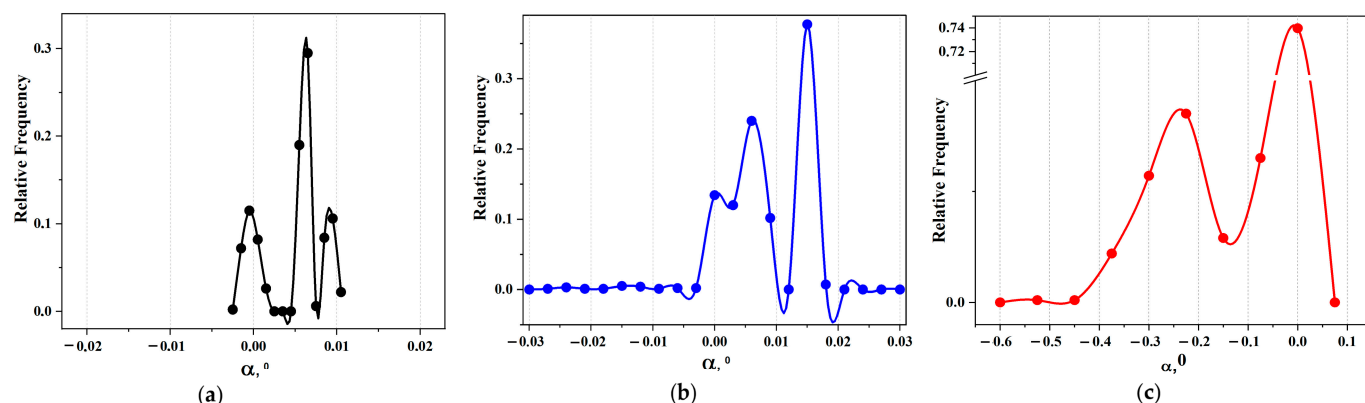


Figure 8. The relative frequency of occurrence as a function of optical rotation angle: (a) water, deuterium-depleted, ≤ 2 ppm; (b) water, bidistilled (SMOW-V); (c) deuterium oxide, 99.8 atom % D(2) ($n = 1000$; $p = 0.95$).

The results clearly demonstrate fluctuations in the angle of optical rotation around zero with a slight shift to the positive region of rotation, while in Bd water corresponding to the SMOW-V standard the region of occurrence of optical rotation is positive, and in the D₂O medium it is mainly negative, occupying a larger magnitude range of rotation angle values.

Thus, the studies of samples with different deuterium contents in water indicate the important role of the heavy stable nucleus of the hydrogen atom in the manifestation of dispersion and optical properties expressed through the ability to rotate and refract light, as well as in the formation of density inhomogeneities in water (water clusters).

3.3. The Validation of the Portable Device to Monitor D/H Ratio in Water Samples

As stated above (see Section Study Design), water (including “ultrapure”) and aqueous solutions are microdisperse systems caused by structural fluctuations and the density of hydrogen bond networks, where the water clusters can cover over 95% of hydrogen bond network, among which some clusters maximally encompass thousands of molecules [65]. In this regard, diffuse reflection of highly coherent laser light from scatterers (periodic structures, clusters) in a smooth surface in a visible wavelength scale contributes to the appearance of optical phase changes and maximum speckle contrast [66].

Single descriptors that maximally reflect the difference between the objects under study were selected (Figure S2) from the entire variety of topological descriptors used for chemometric processing of DSpc, describing the qualitative state of the smooth surface of a water sample with a certain content of stable nuclei of hydrogen atoms. Figure 9 shows the relative frequency of the occurrence of topological descriptor d₂ in the form of a normal Gaussian distribution within the framework of assessing the intra-laboratory precision of the developed technique (using the Bd sample as an example).

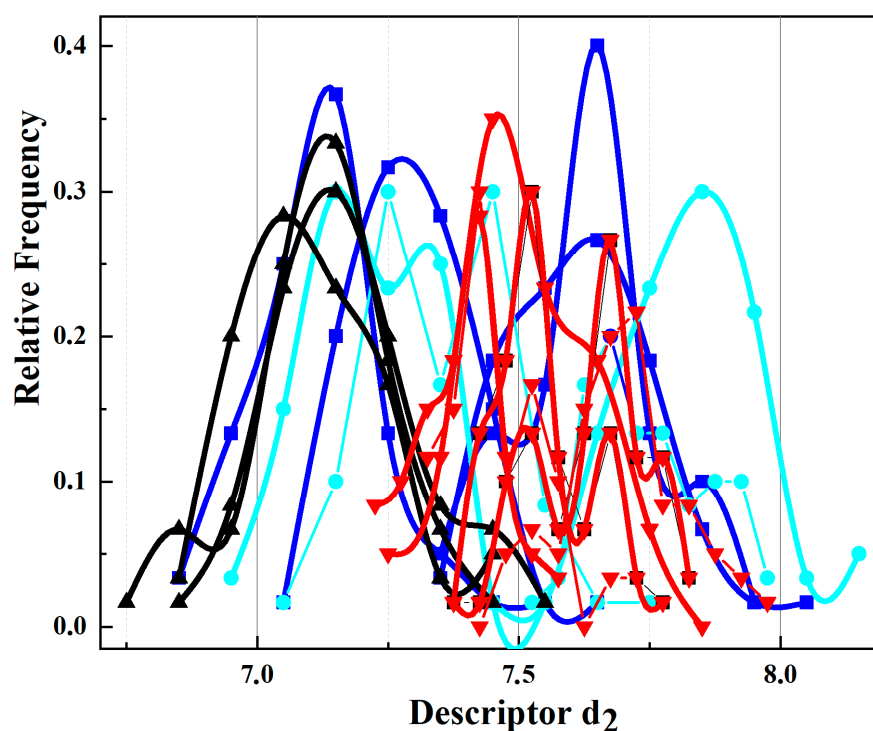


Figure 9. The relative frequency of the occurrence of topological descriptor d₂ of the 2D-DLS method when assessing the intra-laboratory reproducibility of the results of chemometric processing of DSpc structures of Bd samples. RSD for each day: RSD = 3.6% (dark blue curve); RSD = 3.8% (light blue curve); RSD = 2.0% (black curve); RSD = 1.8% (red curve); and intra-laboratory reproducibility RSD = 3.4%.

Statistical processing of DS allows for obtaining information about such parameters as the speed of movement (assembly/decay) of scatterers in the near-surface layer, the amplitude and frequency of their vibrations, etc., where changes may be caused, for example, by the occurrence of stochastic processes.

Figure 10 shows graphical dependence of the family of 2D-DLS topological descriptors on the nature of the aqueous sample with D/H variations, including that within the framework of assessing the intra-laboratory reproducibility (Table 4).

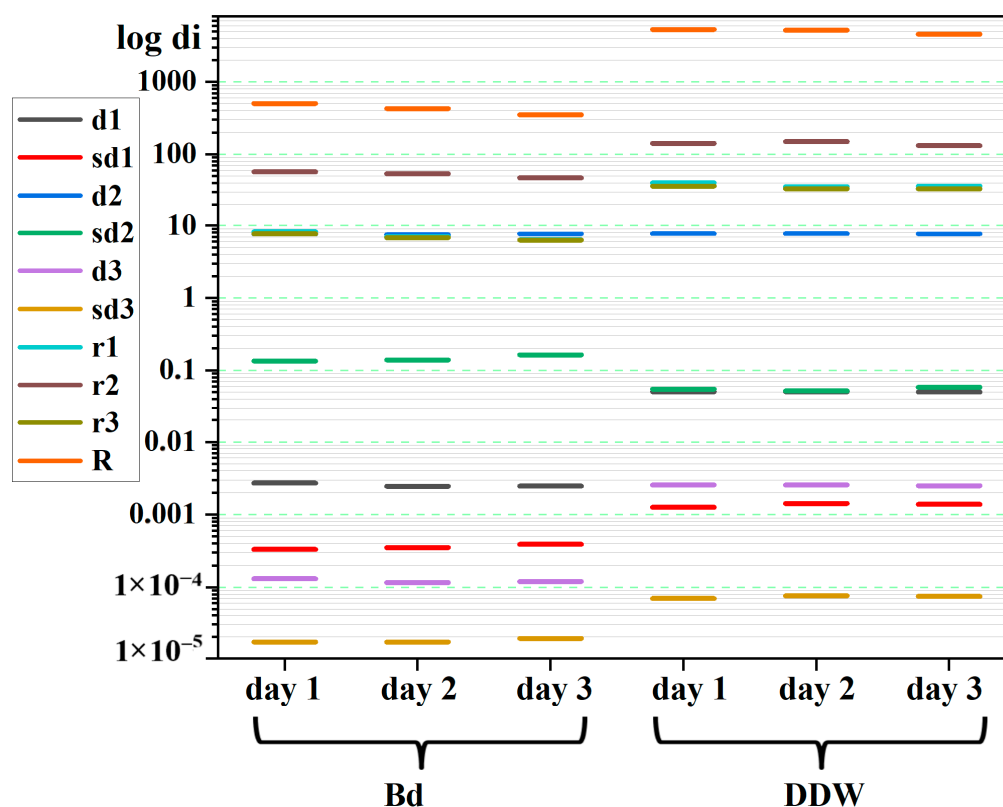


Figure 10. The two-dimensional diagram of the diffuse laser scattering method for water samples with different D/H ratios: water bidistilled (Bd, SMOW-V) and deuterium-depleted water (DDW, ≤ 2 ppm).

Table 4. Validation parameters for linearity of 2D-DLS results in the domain of D/H analyticity.

Linear Dependence Parameters			$y = ax + b$	
Constant (Free) Term, $b \pm SD$	Slope, $a \pm SD$	Coefficient of Determination, (R-Square)	Adjusted R^2	Pearson's Coefficient, r
90.06 ± 13.83	1.37 ± 0.13	0.975 $y = 1.37 \cdot x + 90.063$	0.966	0.987

As can be seen from the presented figure, a set of descriptors in the form of horizontal data-stripes demonstrates the stability of values of the entire family for a specific sample (Bd and DDW), intra-laboratory reproducibility, and differentiation between samples.

The topological descriptor R manifested itself particularly clearly (Figure 11a), which allowed for constructing a linear (calibration) relation “R-D/H, ppm” (Figure 11b, Table S1).

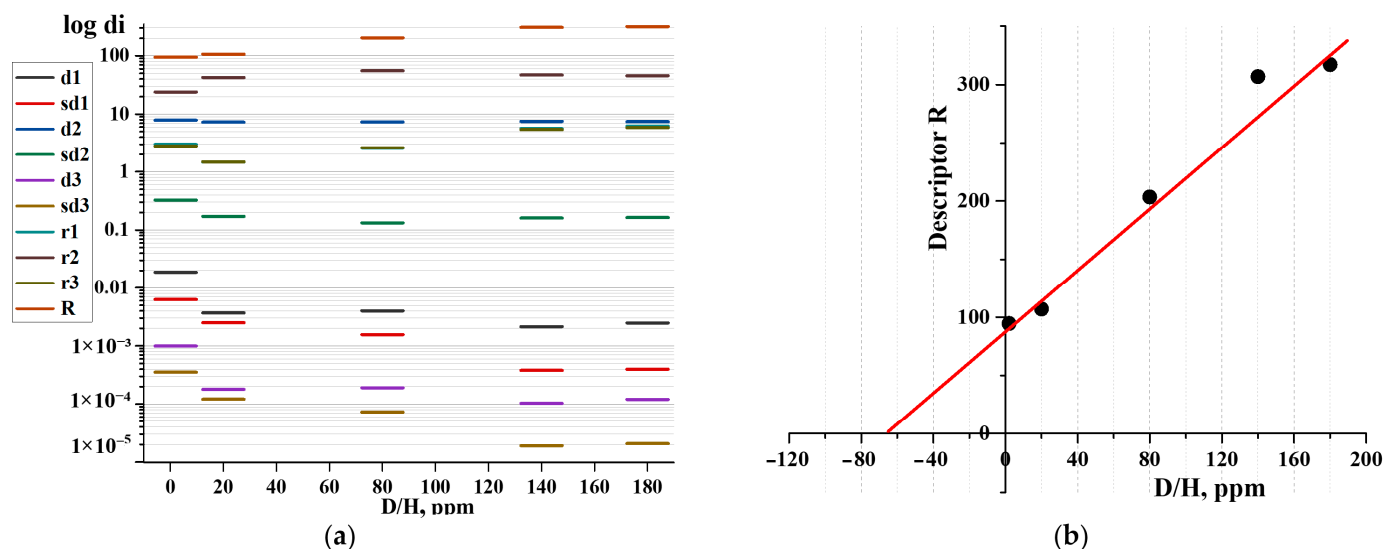


Figure 11. Determining of the intra-laboratory reproducibility of water samples with different D/H ratio results using the 2D-DLS method for a range of laboratory samples with D/H variations from 1 ppm to 180 ppm: (a) the 2D-diagram; (b) the linear dependence in the “descriptor R-D/H, ppm” coordinates.

An analytical range (AR) was established, within which a linear ($r = 0.987$) range was observed, covering the interval between the upper ($D/H \leq 2$ ppm) and lower ($D/H = 180$ ppm) limits for the quantitative determination of stable nuclei of the hydrogen atom in water and aqueous solutions. It was shown that the values of Pearson’s coefficient, R-Square and adjusted R-Square, which serves as the strong linear relation between paired data, a measure to qualify the linear regression and quantify how well the model correlates with the results obtained, are close to 1. Thus, the obtained regression results allow for simulating the ratios between the predicted values based on the developed 2D-DLS model, a fast and simple technique for stable hydrogen nuclide monitoring in aqueous solutions and adjuvant therapeutics.

4. Discussion

The importance of developing innovative solutions in the field of medicine and rehabilitation is undeniable [67]. The trend towards the development and implementation of rapid diagnostic systems and compact measuring devices are increasingly affecting the field of medicine and pharmaceuticals, which is due to the recommendations of the WHO and the International Agency for Research on Cancer (IARC <https://gco.iarc.fr/today/en>, accessed on 25 November 2024) for patient-oriented prevention, early detection, treatment, adjuvant therapy, and palliative care. This article presents the possibilities of a method based on the physical phenomenon of diffuse scattering on the surface of a liquid sample, due to the nature and properties of aqueous deuterium-dependent structures. The article explores the promising directions of the proposed 2D-DLS method: scaling (Figure S3) and expanding the range of deuterium-depleted water preparations to analyses the potential utility of DDW for therapeutic use in phase II clinical trials [68].

5. Conclusions

We have explored the possibility of using a portable dynamic laser speckle technique to detect long-term changes caused by the formation of surface periodic microstructures in water and aqueous solutions. The properties of these structures have been revealed to be influenced by the isotopic composition of water, namely the ratio of heavy and light hydrogen atoms, which have the greatest difference in masses and thus exhibit a noticeable effect in the case of substitution. The developed mobile equipment, which included a compact laser emitter, a test sample, a converging lens, a CCD matrix, and a personal com-

puter with the original software for processing diffuse scattering speckle patterns, showed prospective results. These properties make the devised system particularly interesting for possible in situ determination of deuterium content in water and aqueous adjuvant agents in course of anticancer therapy [32]. The portable equipment can be applied in other areas of expertise to monitor the D/H ratios in the production cycle of deuterium-depleted water. Elimination of the existing drawbacks of the method, such as temperature drift and reduction of analyte volume due to evaporation processes, influence of foreign inhomogeneous particles and external vibrations due to forced temperature control, isolation and other settings of instrumental parameters and measurement modes, will make it possible to eliminate their influence on the suitability of the analytical method and promote its large-scale application [69].

Supplementary Materials: The following supporting information can be downloaded at: <https://www.mdpi.com/article/10.3390/scipharm92040063/s1>, Figure S1: Dependence of the optical angle of rotation on the time in water samples: (a) D₂O, (b) DDW, (c) BD. Figure S2: The diagram of Intra-laboratory reproducibility for Bd water samples ($n = 14$). Figure S3: Portable equipment of diffuse scattered light technology at the production and testing site of the pharmaceutical holding (Russian Federation). Table S1: Chemometric 2D-DLS descriptors of water samples with different D/H ratio.

Author Contributions: Conceptualization, methodology, A.V.S., T.V.P., E.V.U. and O.V.L.; investigation, O.V.L., E.V.U., H.T.N.Q., E.S.K. and I.V.K.; data curation, A.V.S., E.V.U. and O.V.L.; formal analysis, O.V.L.; writing—original draft preparation, E.V.U.; writing—review and editing, A.V.S., E.V.U. and O.V.L. All the authors discussed the results and commented on the manuscript. All authors have read and agreed to the published version of the manuscript.

Funding: the RUDN University Scientific Projects Grant System, project № 033322-2-000, has supported this publication.

Institutional Review Board Statement: Not applicable.

Informed Consent Statement: Not applicable.

Data Availability Statement: The data presented in this study are available in this article and Supplementary Materials.

Conflicts of Interest: The authors declare no conflicts of interest.

Abbreviations

in situ	the original (primary, without movement) location of experiments
Bd	water bidistilled
CCD	charge-coupled device
CAT	catalase
CRM	confocal Raman microscopy
CR	count rate
DDW	deuterium-depleted water
DLS	dynamic light scattering
DSpc	dynamic speckle
DS	diagnostic sign
5-FU	5-fluorouracil
^{obs} E _a	activation energy observed
2D-DLS	two-dimensional diffuse laser scattering
GBM	glioblastoma multiforme
GC/MS	gas chromatography mass spectrometry
GCOS	global climate observing system
GNIR	global network of isotopes in rivers
GNIP	global network of isotopes in precipitation
GISP	Greenland ice sheet precipitation
GRESF	Greenland summit precipitation

G1/S	transition G1 phase ends when the cell moves into the s phase of interphase
MCF-7	Michigan Cancer Foundation-7
OR	optical rotation
IAEA	international atomic energy agency
IR	infra-red
IR-MS	isotope ratio mass spectrometers
IRIS	isotope ratio infrared spectroscopy
LED	light-emitting diode
LC/MS	liquid chromatography mass spectrometry
LAP	standard Light Antarctic Precipitation
LALLS	low-angle laser light scattering
PSD	particle size distribution
ppm	part per million
PDI	polydispersity Index
RI	refractive index
QSAR	quantitative structure–activity relationship
RT	radiation therapy
SMOW-V	Vienna standard mean ocean water
SNR	signal to noise ratio
SOD	superoxide dismutase
TMZ	temozolomide

References

- Hughes, J. Making isotopes matter: Francis Aston and the mass-spectrograph December. *Dynamis* **2009**, *29*, 131–165. [\[CrossRef\]](#)
- Harold, C.; Urey, F.G.; Brickwedde, G.M.; Murphy, A. Hydrogen Isotope of Mass 2 and its Concentration. *Phys. Rev.* **1932**, *40*, 1.
- Watanabe, H.; Lorusso, G.; Nishimura, S.; Xu, Z.Y.; Sumikama, T.; Söderström, P.A.; Doornenbal, P.; Browne, F.; Gey, G.; Jung, H.S. Isomers in 128Pd and 126Pd: Evidence for a robust shell closure at the neutron magic number 82 in exotic palladium isotopes. *Phys. Rev.* **2013**, *111*, 152501.
- Yang, H.B. Discovery of new isotopes 160Os and 156W: Revealing enhanced stability of the N = 82 shell closure on the neutron-deficient side. *Phys. Rev. Lett.* **2024**, *132*, 072502. [\[CrossRef\]](#)
- Radchenko, V.; Morgenstern, A.; Jalilian, A.R.; Ramogida, C.F.; Cutler, C.; Duchemin, C.; Hoeher, C.; Haddad, F.; Bruchertseifer, F.; Gausemel, H.; et al. Production and Supply of α -Particle-Emitting Radionuclides for Targeted α -Therapy. *J. Nucl. Med.* **2021**, *62*, 1495–1503. [\[CrossRef\]](#)
- Carpentier, A.C. Tracers and Imaging of Fatty Acid and Energy Metabolism of Human Adipose Tissues. *Physiology* **2024**, *39*, 61–72. [\[CrossRef\]](#)
- Wilkinson, D.J.; Crossland, H.; Atherton, P.J. Metabolomic and proteomic applications to exercise biomedicine. *Transl. Exerc. Biomed.* **2024**, *1*, 9–22. [\[CrossRef\]](#)
- Brook, M.S.; Wilkinson, D.J. Contemporary stable isotope tracer approaches: Insights into skeletal muscle metabolism in health and disease. *Exp. Physiol.* **2020**, *105*, 1081–1089. [\[CrossRef\]](#)
- Kim, I.Y.; Suh, S.H.; Lee, I.K. Applications of stable, nonradioactive isotope tracers in in vivo human metabolic research. *Exp. Mol. Med.* **2016**, *48*, e203. [\[CrossRef\]](#)
- Wolfe, R.R.; Chinkes, D.L. *Isotope Tracers in Metabolic Research*, 2nd ed.; John Wiley & Sons, Inc.: Hoboken, NJ, USA, 2005.
- Wilkinson, D.J.; Brook, M.S.; Smith, K.; Atherton, P.J. Stable isotope tracers and exercise physiology: Past, present and future. *J. Physiol.* **2017**, *595*, 2873–2882. [\[CrossRef\]](#)
- Meija, J.; Coplen, T.B.; Michael, B.; Willi, A.B.; De Bièvre, P.; Manfred, G.; Holden, N.E.; Johanna, I.; Loss, R.D.; Walczyk, T.; et al. Isotopic compositions of the elements 2013. *Pure Appl. Chem.* **2016**, *88*, 293–306. [\[CrossRef\]](#)
- O’Grady, S.P.; Valenzuela, L.O.; Remien, C.H.; Enright, L.E.; Jorgensen, M.J.; Kaplan, J.R.; Wagner, J.D.; Cerling, T.E.; Ehleringer, J.R. Hydrogen and oxygen isotope ratios in body water and hair: Modeling isotope dynamics in nonhuman primates. *Am. J. Primatol.* **2012**, *74*, 651–660. [\[CrossRef\]](#) [\[PubMed\]](#)
- Abudouwaili, Z.; Yang, Y.; Feng, X. Characteristics of Hydrogen–Oxygen Isotopes and Water Vapor Sources of Different Waters in the Ili Kashi River Basin. *Water* **2023**, *15*, 3127. [\[CrossRef\]](#)
- Borodulina, G.; Tokarev, I.; Yakovlev, E. Isotope Composition of Natural Water in Lake Onega Basin. *Water* **2023**, *15*, 1855. [\[CrossRef\]](#)
- Groning, M.; Van Duren, M.; Andreescu, L. Metrological Characteristics of the Conventional Measurement Scales for Hydrogen and Oxygen Stable Isotope Amount Ratios: The δ -Scales. In *Combining and Reporting Analytical Results*; Belli, M., Fajgelj, A., Sansone, U., Eds.; The Royal Society of Chemistry: London, UK, 2007; pp. 62–72.
- Valenzuela, L.O.; O’Grady, S.P.; Ehleringer, J.R. Variations in human body water isotope composition across the United States. *Forensic Sci. Int.* **2021**, *327*, 110990. [\[CrossRef\]](#)

18. Su, Y.; Otake, K.; Zheng, J.J.; Satoshi, H.; Susumu, K.; Cheng, G. Separating water isotopologues using diffusion-regulatory porous materials. *Nature* **2022**, *611*, 289–294. [\[CrossRef\]](#)
19. Basov, A.; Fedulova, L.; Baryshev, M.; Dzhimak, S. Deuterium-Depleted Water Influence on the Isotope $^2\text{H}/^1\text{H}$ Regulation in Body and Individual Adaptation. *Nutrients* **2019**, *11*, 1903. [\[CrossRef\]](#)
20. Rea, E. The Theory of Relativity and Applications: A Simple Introduction. *Downt. Rev.* **2018**, *5*, 1.
21. Jasprica, I.; Horvat, P.; Zrnc, K.; Bonney, K.J.; Bjornstad, V.; Hok, L.; Vianello, R.; Bregović, N.; Požar, J.; Leko, K.; et al. Utilization of a kinetic isotope effect to decrease decomposition of ceftriaxone in a mixture of $\text{D}_2\text{O}/\text{H}_2\text{O}$. *Eur. J. Pharm. Sci.* **2023**, *187*, 106461. [\[CrossRef\]](#)
22. Lu, Y.; Chen, H. Deuterium-Depleted Water in Cancer Therapy: A Systematic Review of Clinical and Experimental Trials. *Nutrients* **2024**, *16*, 1397. [\[CrossRef\]](#)
23. Zlatkiy, I.; Pleteneva, T.; Skripnikov, A.; Grebennikova, T.; Maksimova, T.; Antipova, N.; Levitskaya, O.; Makarova, M.; Selivanenko, I.; Syroeshkin, A. Dependence of Biocatalysis on D/H Ratio: Possible Fundamental Differences for High-Level Biological Taxons. *Molecules* **2020**, *25*, 4173. [\[CrossRef\]](#) [\[PubMed\]](#)
24. Jandova, J.; Hua, A.B.; Fimbres, J.; Wondrak, G.T. Deuterium Oxide (D_2O) Induces Early Stress Response Gene Expression and Impairs Growth and Metastasis of Experimental Malignant Melanoma. *Cancers* **2021**, *13*, 605. [\[CrossRef\]](#) [\[PubMed\]](#)
25. Yaglova, N.V.; Timokhina, E.P.; Obernikhin, S.S.; Yaglov, V.V. Emerging Role of Deuterium/Protium Disbalance in Cell Cycle and Apoptosis. *Int. J. Mol. Sci.* **2023**, *24*, 3107. [\[CrossRef\]](#) [\[PubMed\]](#)
26. Kselíková, V.; Vítová, M.; Bišová, K. Deuterium and its impact on living organisms. *Folia Microbiol.* **2019**, *64*, 673–681. [\[CrossRef\]](#)
27. Somlyai, G.; Jancso, G. Naturally occurring deuterium is essential for the normal growth rate of cells. *FEBS Lett.* **1993**, *7*, 344–366. [\[CrossRef\]](#)
28. Kharaeva, Z.; Hokonova, T.; Elmurzaeva, J.; Dzamihova, I.; Mayer, W.; De Luca, C.; Trakhtman, I.; Korkina, L. Effects of Heavy Isotopes ($^2\text{H}_1$ and $^{18}\text{O}_{16}$) Depleted Water Consumption on Physical Recovery and Metabolic and Immunological Parameters of Healthy Volunteers under Regular Fitness Load. *Sports* **2021**, *9*, 110. [\[CrossRef\]](#)
29. Wang, H.; Zhu, B.; He, Z.; Fu, H.; Dai, Z.; Huang, G.; Li, B.; Qin, D.; Zhang, X.; Tian, L.; et al. Deuterium-depleted water (DDW) inhibits the proliferation and migration of nasopharyngeal carcinoma cells in vitro. *Biomed. Pharmacother.* **2013**, *67*, 489–496. [\[CrossRef\]](#)
30. Somlyai, G.; Kovács, B.Z.; Papp, A.; Somlyai, I. A Preliminary Study Indicating Improvement in the Median Survival Time of Glioblastoma Multiforme Patients by the Application of Deuterium Depletion in Combination with Conventional Therapy. *Biomedicines* **2023**, *11*, 1989. [\[CrossRef\]](#)
31. Boros, L.G.; Somlyai, I.; Kovács, B.Z.; Puskás, L.G.; Nagy, L.I.; Dux, L.; Farkas, G.; Somlyai, G. Deuterium Depletion Inhibits Cell Proliferation, RNA and Nuclear Membrane Turnover to Enhance Survival in Pancreatic Cancer. *Cancer Control* **2021**, *28*, 1073274821999655. [\[CrossRef\]](#)
32. Yavari, K.; Kooshesh, L. Deuterium Depleted Water Inhibits the Proliferation of Human MCF7 Breast Cancer Cell Lines by Inducing Cell Cycle Arrest. *Nutr. Cancer* **2019**, *71*, 1019–1029. [\[CrossRef\]](#)
33. Wang, H.; Liu, C.; Fang, W.; Yang, H. Research progress of the inhibitory effect of deuterium-depleted water on cancers. *J. South Med. Univ.* **2012**, *32*, 1454–1456.
34. Somlyai, G.; Kovács, B.Z.; Somlyai, I.; Papp, A.; Nagy, L.I.; Puskás, L.G. Deuterium depletion inhibits lung cancer cell growth and migration in vitro and results in severalfold increase of median survival time of non-small cell lung cancer patients receiving conventional therapy. *J. Cancer Res. Ther.* **2021**, *9*, 12–19.
35. Kovács, B.Z.; Papp, A.; Somlyai, I.; Somlyai, G. Long-term survival rates of cancer patients achieved by deuterium depletion as an adjuvant treatment in spinal astrocytic glioma, carcinoma mammae and melanoma malignum. *Clin. Med. Case Rep.* **2023**, *9*, 2121.
36. Zhang, X.; Gaetani, M.; Chernobrovkin, A.; Zubarev, R. Anticancer Effect of Deuterium Depleted Water - Redox Disbalance Leads to Oxidative Stress. *Mol. Cell. Proteom.* **2019**, *18*, 2373–2387. [\[CrossRef\]](#)
37. Davoudpour, Y.; Kümmel, S.; Musat, N.; Richnow, H.H.; Schmidt, M. Tracking deuterium uptake in hydroponically grown maize roots using correlative helium ion microscopy and Raman micro-spectroscopy. *Plant Methods* **2023**, *19*, 71. [\[CrossRef\]](#)
38. Ankner, J.F.; Heller, W.T.; Herwig, K.W.; Meilleur, F.; Myles, D.A. Neutron scattering techniques and applications in structural biology. *Curr. Protoc. Protein Sci.* **2013**, *17*, 16. [\[CrossRef\]](#)
39. Wang, L.; Caylor, K.K.; Dragoni, D. On the calibration of continuous, high-precision $\delta^{18}\text{O}$ and $\delta^2\text{H}$ measurements using an off-axis integrated cavity output spectrometer. *Rapid Commun. Mass Spectrom.* **2009**, *23*, 530–536. [\[CrossRef\]](#)
40. Adsiz, C.; Skrzypek, G.; McCallum, J. The measurement of ambient air moisture stable isotope composition for the accurate estimation of evaporative losses. *MethodsX* **2023**, *11*, 102265. [\[CrossRef\]](#)
41. Steele, Z.T.; Caceres, K.; Jameson, A.D.; Griego, M.; Rogers, E.J.; Whiteman, J.P. A protocol for distilling animal body water from biological samples and measuring oxygen and hydrogen stable isotopes via cavity ring-down spectroscopy. *Isotopes Environ. Health Stud.* **2024**, *12*, 3. [\[CrossRef\]](#)
42. Fisher Scientific. Available online: <https://www.fishersci.com/shop/products/deuterium-oxide-nmr-99-8-atom-d-acroscial-thermo-scientific/AC426931000> (accessed on 21 June 2024).
43. Bethesda (MD): National Library of Medicine (US), National Center for Biotechnology Information; PubChem Compound Summary for CID 962, Water. Available online: <https://pubchem.ncbi.nlm.nih.gov/compound/Water> (accessed on 21 June 2024).
44. Haynes, W.M. *CRC Handbook of Chemistry and Physics*, 94th ed.; CRC: Boca Raton, FL, USA; London, UK, 2012; pp. 4–98.

45. Goncharuk, V.V.; Pleteneva, T.V.; Grebennikova, T.V.; Syroeshkin, A.V.; Uspenskaya, E.V.; Antipova, N.V.; Kovalenko, V.F.; Saprykina, M.N.; Skliskaya, M.D.; Zlatskiy, I.A. Determination of Biological Activity of Water Having a Different Isotope Ratio of Protium and Deuterium. *J. Water Chem. Technol.* **2018**, *40*, 27–34. [\[CrossRef\]](#)
46. Baek, Y.; Lee, K.; Oh, J.; Park, Y. Speckle-Correlation Scattering Matrix Approaches for Imaging and Sensing through Turbidity. *Sensors* **2020**, *20*, 3147. [\[CrossRef\]](#) [\[PubMed\]](#)
47. Lee, K.; Park, Y. Interpreting Intensity Speckle as the Coherency Matrix of Classical Light. *Phys. Rev. Appl.* **2019**, *12*, 024003. [\[CrossRef\]](#)
48. Zhang, H.; Hu, Y.; Peng, S.; Liu, Y. Study on Speckle Noise Reduction in Laser Projection Displays. *Photonics* **2024**, *11*, 290. [\[CrossRef\]](#)
49. Pérez, A.J.; González-Peña, R.J.; Braga, R., Jr.; Perles, Á.; Pérez-Marín, E.; García-Diego, F.J. A Portable Dynamic Laser Speckle System for Sensing Long-Term Changes Caused by Treatments in Painting Conservation. *Sensors* **2018**, *18*, 190. [\[CrossRef\]](#) [\[PubMed\]](#)
50. Schnars, U.; Falldorf, C.; Watson, J.; Jüptner, W. *Digital Holography and Wavefront Sensing*; Springer: Berlin/Heidelberg, Germany, 2015.
51. Kim, M.K. Principles and techniques of digital holographic microscopy. *SPIE Rev.* **2010**, *1*, 018005. [\[CrossRef\]](#)
52. Bunkin, N.F.; Shkirin, A.V.; Babenko, V.A.; Sychev, A.A.; Lomkova, A.K.; Kulikov, E.S. Laser diagnostics of the Bubston phase in the bulk of aqueous salt solutions. *Phys. Wave Phen.* **2015**, *23*, 161–175. [\[CrossRef\]](#)
53. Yurchenko, S.O.; Shkirin, A.V.; Ninham, B.W.; Sychev, A.A.; Babenko, V.A.; Penkov, N.V.; Kryuchkov, N.P.; Bunkin, N.F. Ion-Specific and Thermal Effects in the Stabilization of the Gas Nanobubble Phase in Bulk Aqueous Electrolyte Solutions. *Langmuir* **2016**, *32*, 11245–11255. [\[CrossRef\]](#)
54. Goncharuk, V.V.; Syroeshkin, A.V.; Pleteneva, T.V.; Uspenskaya, E.V.; Levitskaya, O.V.; Tverdislov, V.A. On the possibility of chiral structure-density submillimeter inhomogeneities existing in water. *J. Water Chem. Technol.* **2017**, *39*, 319–324. [\[CrossRef\]](#)
55. Fusi, L.; Farina, A.; Rosso, F.; Rajagopal, K. Thin-Film Flow of an Inhomogeneous Fluid with Density-Dependent Viscosity. *Fluids* **2019**, *4*, 30. [\[CrossRef\]](#)
56. Kovalenko, K.V.; Krivokhizha, S.V.; Chaban, I.A. Detection of various phases in liquids from the hypersound velocity and damping near closed phase-separation regions of solutions. *J. Exp. Theor. Phys.* **2008**, *106*, 280–287. [\[CrossRef\]](#)
57. Bunkin, N.; Sabirov, L.; Semenov, D.; Ismailov, F.; Khasanov, M. Nanoscale Structural Phase Transitions in Aqueous Solutions of Organic Molecules. *Condens. Matter* **2023**, *8*, 64. [\[CrossRef\]](#)
58. Anand, M.; Rajagopal, K. A note on the flows of inhomogeneous fluids with shear-dependent viscosities. *Arch. Mech.* **2005**, *57*, 417–428.
59. Rajagopal, K.; Srinivasa, A. Modeling anisotropic fluids within the frame- work of bodies with multiple natural configurations. *J. Non-Newt. Fluid Mech.* **2001**, *99*, 109–124. [\[CrossRef\]](#)
60. Yakhno, T.; Yakhno, V. A Study of the Structural Organization of Water and Aqueous Solutions by Means of Optical Microscopy. *Crystals* **2019**, *9*, 52. [\[CrossRef\]](#)
61. Goncharuk, V.V.; Lapshin, V.B.; Burdeinaya, T.N.; Pleteneva, T.V.; Chernopyatko, A.S.; Atamanenko, I.D.; Ul'yantsev, A.S.; Uspenskaya, E.V.; Todorov, A.O.; Taranov, V.V.; et al. Physicochemical Properties and Biological Activity of the Water Depleted of Heavy Isotopes. *J. Water Chem. Technol.* **2011**, *33*, 8–13. [\[CrossRef\]](#)
62. Koldina, A.M.; Uspenskaya, E.V.; Borodin, A.A.; Pleteneva, T.V.; Syroeshkin, A.V. Light scattering in research and quality control of deuterium depleted water for pharmaceutical application. *Int. J. Appl. Pharm.* **2019**, *11*, 271–278. [\[CrossRef\]](#)
63. Bunkin, N.F.; Shkirin, A.V.; Kozlov, V.A.; Ninham, B.W.; Uspenskaya, E.V.; Gudkov, S.V. Near-surface structure of Nafion in deuterated water. *J. Chem. Phys.* **2018**, *149*, 164901. [\[CrossRef\]](#)
64. Gao, Y.; Fang, H.; Ni, K. Water clusters and density fluctuations in liquid water based on extended hierarchical clustering methods. *Sci. Rep.* **2022**, *12*, 8036. [\[CrossRef\]](#)
65. Gao, Y.; Fang, H.; Ni, K. A hierarchical clustering method of hydrogen bond networks in liquid water undergoing shear flow. *Sci. Rep.* **2021**, *11*, 9542. [\[CrossRef\]](#)
66. Nilsson, A.; Pettersson, L.G.M. Perspective on the structure of liquid water. *Chem. Phys.* **2011**, *389*, 1–34. [\[CrossRef\]](#)
67. Ochoa, E.; Goodman, J.W. Statistical properties of ray directions in a monochromatic speckle pattern. *JOSA* **1983**, *73*, 943–949. [\[CrossRef\]](#)
68. Galić, I.; Habijan, M.; Leventić, H.; Romić, K. Machine Learning Empowering Personalized Medicine: A Comprehensive Review of Medical Image Analysis Methods. *Electronics* **2023**, *12*, 4411. [\[CrossRef\]](#)
69. Liu, M.; Han, Y.; Xi, X.; Zhu, L.; Yang, S.; Tan, S.; Chen, J.; Li, L.; Yan, B. Multiscale Dense U-Net: A Fast Correction Method for Thermal Drift Artifacts in Laboratory NanoCT Scans of Semi-Conductor Chips. *Entropy* **2022**, *24*, 967. [\[CrossRef\]](#) [\[PubMed\]](#)

Disclaimer/Publisher's Note: The statements, opinions and data contained in all publications are solely those of the individual author(s) and contributor(s) and not of MDPI and/or the editor(s). MDPI and/or the editor(s) disclaim responsibility for any injury to people or property resulting from any ideas, methods, instructions or products referred to in the content.